Simple loss-tolerant protocol for Greenberger-Horne-Zeilinger-state distribution in a quantum network

Shimizu, Hikaru; Roga, Wojciech; Elkouss, David; Takeoka, Masahiro

DOI
10.1103/PhysRevA.111.022624

Publication date
2025

Document Version
Final published version

Published in
Physical Review A

Simple loss-tolerant protocol for Greenberger-Horne-Zeilinger-state distribution in a quantum network

Hikaru Shimizu [1,*] Wojciech Roga [1,†] David Elkouss [2,3,‡] and Masahiro Takeoka [1,4,§]

[1]*Department of Electronics and Electrical Engineering, Keio University, 3-14-1 Hiyoshi, Kohoku-ku, Yokohama 223-8522, Japan*
[2]*Networked Quantum Devices Unit, Okinawa Institute of Science and Technology Graduate University, Okinawa, Japan*
[3]*QuTech, Delft University of Technology, Lorentzweg 1, 2628 CJ Delft, The Netherlands*
[4]*National Institute of Information and Communications Technology (NICT), Koganei, Tokyo 184-8795, Japan*

(Received 2 May 2024; revised 27 September 2024; accepted 23 January 2025; published 21 February 2025)

Distributed quantum entanglement plays a crucial role in realizing networks that connect quantum devices. However, sharing entanglement between distant nodes by means of photons is a challenging process primary due to unavoidable losses in the linking channels. In this paper, we propose a simple loss-tolerant protocol for the Greenberger-Horne-Zeilinger-state distribution. We analyze the distribution rate under feasible experimental conditions and demonstrate the advantages of rate-loss scaling with respect to direct transmission. Our protocol does not use quantum repeaters and is achievable with current quantum optics technology. The result has direct application to tasks such as conference key agreement or distributed sensing. Moreover, it reduces the requirements for implementing distributed quantum error correction codes such as the surface code.

DOI: 10.1103/PhysRevA.111.022624

I. INTRODUCTION

Quantum links allow distant nodes to be connected in quantum networks [1–3], which are expected to impact such fields as cryptography [4–8], high accuracy clock synchronization [9], longer-baseline telescopes [10,11], quantum sensing [12–15], and quantum computing [16,17]. In quantum networks, users can exchange arbitrary quantum states between distant nodes through quantum teleportation [18], which consumes shared entanglement. Therefore, bipartite entanglement distribution is one of the most important processes for quantum networks. Multipartite entanglement was often distilled from copies of the bipartite one and became a standard procedure both in experimental and theoretical studies. However, generating multipartite entangled states directly, also showed advantages in specific cases [19,20].

In typical networks, quantum entanglement is shared by means of transmitted photons. Considering star networks, as in Fig. 1, the simplest protocol distributing multipartite entanglement consists of generating a desired quantum state locally at the central node and transmitting it by photons to each user node as in Fig. 1(a). This solution was demonstrated experimentally [7] and proven feasible, however, its efficiency was strongly limited by the photon loss. Indeed, here, N photons, where N is the number of end-node users, must simultaneously successfully survive transmission through the lossy channels. Therefore, the distribution rate scales as $O(\eta^N)$, where η is the probability that one photon successfully passes through the channel of a given length [21,22]. This protocol is referred to as the "direct transmission protocol" due to the absence of any repeater-like operations. In principle, a perfect quantum repeater with quantum memory at the central node can be implemented in a protocol achieving the distribution rate that scales as $O(\eta)$ and high fidelity [23–29]. However, although quantum repeaters technology, for instance, with diamond centers or ion trap-based memories, has made significant progress in recent years and some experimental demonstrations have been performed [30–32], its implementation in multipartite scenarios was still beyond the reach of current technology. Indeed, even two-party implementationwas still challenging. Therefore, how to achieve an advantageous multipartite entanglement generation rate without preshared Bell pairs and quantum memory in fully optical setup with current technology remains a major, unsolved issue which we address in this paper.

In [33] the authors proposed a simple loss-tolerant protocol to distribute the M-photon N-mode Dicke states

$$|D(N,M)\rangle = \frac{1}{\sqrt{{}^{N}C_M}} \sum_{i=1}^{{}^{N}C_M} \left|f_i^{(N,M)}\right\rangle, \tag{1}$$

where ${}^{N}C_M$ is the number of combinations and $|f_i^{(N,M)}\rangle$ are states with N modes and M photons, such that there is, at most, one photon per mode. The authors showed a protocol with rate loss scaling $O(\eta^M)$. It was, however, not known if it could be generalized to generate stronger correlated states like the Greenberger-Horne-Zeilinger (GHZ) state defined as a superposition of two terms perfectly anticorrelated in each of N subsystems

$$|\mathrm{GHZ}\rangle_N = \frac{1}{\sqrt{2}}(|000\ldots0\rangle + |111\ldots1\rangle), \tag{2}$$

*Contact author: shimihika2357@keio.jp
†Contact author: wojciech.roga@keio.jp
‡Contact author: david.elkouss@oist.jp
§Contact author: takeoka@elec.keio.ac.jp

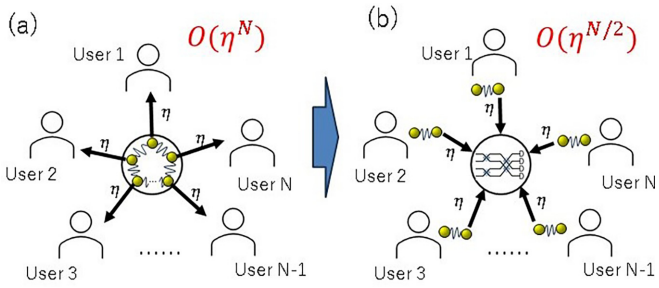

FIG. 1. Generating multipartite entangled states in a star network. (a) Direct transmission protocol. (b) Proposed protocol with appropriate interference and conditional measurement in the central node. Black lines indicate optical fibers of equal length. η is the transmittance of the links.

or the equivalent form with a different basis [e.g., Eq. (3)]. GHZ states are of capital importance for tasks such as conference key agreement [7,8] or quantum sensing [12–15]. The setup from [33] could not generate GHZ states with $N > 4$ producing always more than two terms in Eq. (2). Furthermore, previous studies have not shown that this setup can project the input state to the GHZ states when $N = 4$. In the present paper, we show that it is possible to design an alternative setup in which unwanted terms destructively interfere. We establish an alternative specific protocol, and investigate its performance under realistic experimental conditions. Namely, we calculate the rate and fidelity of GHZ states' generation in a star network considering realistic accessible sources and imperfections of measurement devices. We show that our protocol significantly beats the direct transmission protocol. Note that, although for a given rate, the achievable fidelity may be smaller compared to the memory-based protocols [29] assuming that the quantum state can be stored for a long time and manipulated in the central node, its advantage lies in feasibility with existing quantum optical technology. Our protocol has an immediate impact on well-known protocols based on the GHZ states. Moreover, we propose its application to improve the implementation of stabilizer codes between distributed qubit memories.

II. PROTOCOL

A. Four-partite GHZ-state distribution

In this subsection, we discuss how to distribute a four-partite GHZ state

$$|\mathrm{GHZ}\rangle_4 = \frac{1}{\sqrt{2}}\left(|1010\rangle_{X_1X_2X_3X_4} + |0101\rangle_{X_1X_2X_3X_4}\right), \tag{3}$$

where the indexes indicate the users, $|1\rangle$ denotes one photon, and $|0\rangle$ denotes a vacuum. Note that the state Eq. (3) has the same entanglement properties as that of the standard form of GHZ states in Eq. (2) and thus is directly useful for applications. For the sake of clarity of the presentation, we assume no loss. The scenario with losses and other imperfections is discussed in the next subsection.

Consider a star network, as in Fig. 1, with four users equally distant from the central node. We assume that each user locally generates the state

$$|\psi\rangle_{X_iX_i'} = a|00\rangle_{X_iX_i'} + b|11\rangle_{X_iX_i'}, \tag{4}$$

where $|a|^2 + |b|^2 = 1$. Here, X_i and X_i' denote the subsystems retained by the ith user node, which may be photonic or atomic system, and transmitted to the central node, the flying qubit in a photon number basis, respectively. At the central node, the flying qubits interfere with each other, after which a measurement in the photon number basis is performed. The goal is to find an optical circuit which makes flying qubits interfere appropriately to conditionally transform the retained qubits into the GHZ state depending on the result of the central node measurement. The role of the central node resembles that of the Bell-state measurement [34] in entanglement swapping.

The initial state of the entire system can be described as the product

$$\begin{aligned}\bigotimes_{i=1}^{4}|\psi\rangle_{X_iX_i'} &= \bigotimes_{i=1}^{4}\left(a|00\rangle_{X_iX_i'} + b|11\rangle_{X_iX_i'}\right)\\ &= |\Psi\rangle_{X_1X_2X_3X_4X_1'X_2'X_3'X_4}.\end{aligned} \tag{5}$$

At the central node, the subsystem $X_1' \ldots X_4'$ undergoes a unitary transformation induced by the four-mode circuit [Fig. 2(a)] and is measured by a ray of photon detectors. The circuit consists of two rays of half beam splitters. Each beams plitter is described as a unitary transformation of the input photon creation operators

$$U_{\mathrm{HBS}} = \frac{1}{\sqrt{2}}\begin{bmatrix}1 & 1\\ 1 & -1\end{bmatrix}. \tag{6}$$

If we denote the input and output modes creation operators as $a_i^\dagger$ and $b_i^\dagger$, respectively, the transformation induced by the circuit is

$$\begin{bmatrix}a_1^\dagger\\ a_2^\dagger\\ a_3^\dagger\\ a_4^\dagger\end{bmatrix} = U_{\mathrm{4mc}}^\dagger \begin{bmatrix}b_1^\dagger\\ b_2^\dagger\\ b_3^\dagger\\ b_4^\dagger\end{bmatrix}, \tag{7}$$

where

$$U_{\mathrm{4mc}} = U_{\mathrm{HBS}} \otimes U_{\mathrm{HBS}} = \frac{1}{2}\begin{bmatrix}1 & 1 & 1 & 1\\ 1 & -1 & 1 & -1\\ 1 & 1 & -1 & -1\\ 1 & -1 & -1 & 1\end{bmatrix}. \tag{8}$$

We obtain state Eq. (3) at the user nodes when only two photons arrive at the central node and are detected by appropriate pair of detectors. There are ${}^4C_2 = 6$ terms in the shared subsystems $X_1' \ldots X_4'$ of the input state Eq. (5) that contain two photons. These terms are transformed by the four-mode circuit

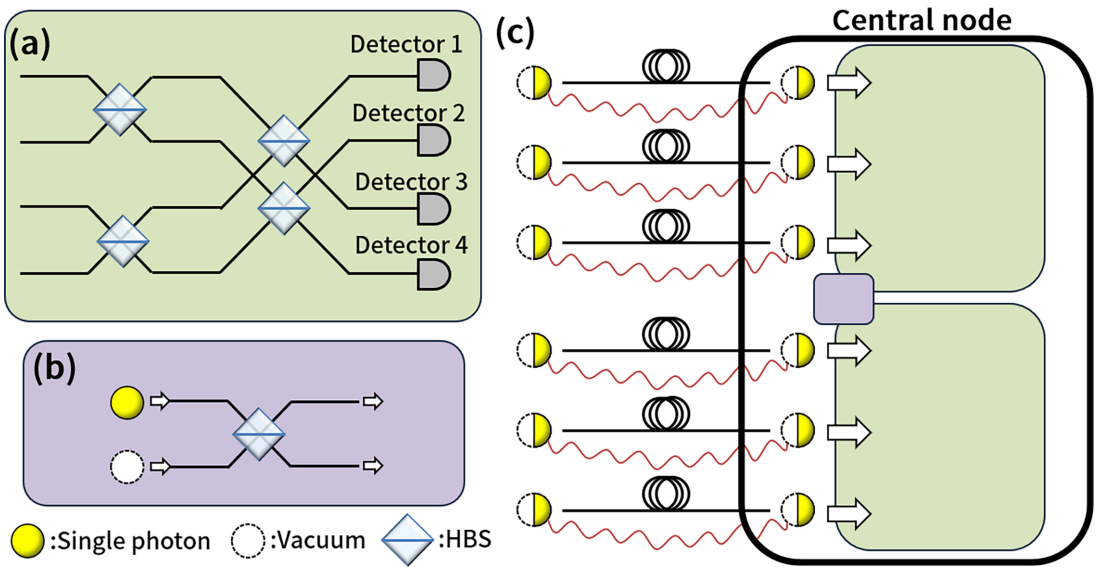

FIG. 2. (a) Central node four-mode circuit generating state $|\mathrm{GHZ}\rangle_4$ in users' nodes $X_1, \ldots, X_4$ when specific pair of bucket detectors detect photons. (c) Central node circuit generating $|\mathrm{GHZ}\rangle_6$ at users' nodes when specific configuration of four bucket detectors detect photons. The central node uses adjacent modes of (a) building blocks and (b) single-photon source to connect the blocks. The setup can be extended to generate $|\mathrm{GHZ}\rangle_N$ with arbitrary N by adding further building blocks and connect their adjacent modes analogously.

at the central node as follows:

$$
\begin{aligned}
&a_1^\dagger a_2^\dagger|0000\rangle_{\mathrm{in}} \\
&\quad\to \tfrac{1}{4}\big(b_1^{\dagger 2}-b_2^{\dagger 2}+b_3^{\dagger 2}-b_4^{\dagger 2}+2b_1^\dagger b_3^\dagger-2b_2^\dagger b_4^\dagger\big)|0000\rangle_{\mathrm{out}} \\
&a_1^\dagger a_3^\dagger|0000\rangle_{\mathrm{in}} \\
&\quad\to \tfrac{1}{4}\big(b_1^{\dagger 2}+b_2^{\dagger 2}-b_3^{\dagger 2}-b_4^{\dagger 2}+2b_1^\dagger b_2^\dagger-2b_3^\dagger b_4^\dagger\big)|0000\rangle_{\mathrm{out}} \\
&a_1^\dagger a_4^\dagger|0000\rangle_{\mathrm{in}} \\
&\quad\to \tfrac{1}{4}\big(b_1^{\dagger 2}-b_2^{\dagger 2}-b_3^{\dagger 2}+b_4^{\dagger 2}+2b_1^\dagger b_4^\dagger-2b_2^\dagger b_3^\dagger\big)|0000\rangle_{\mathrm{out}} \\
&a_2^\dagger a_3^\dagger|0000\rangle_{\mathrm{in}} \\
&\quad\to \tfrac{1}{4}\big(b_1^{\dagger 2}-b_2^{\dagger 2}-b_3^{\dagger 2}+b_4^{\dagger 2}-2b_1^\dagger b_4^\dagger+2b_2^\dagger b_3^\dagger\big)|0000\rangle_{\mathrm{out}} \\
&a_2^\dagger a_4^\dagger|0000\rangle_{\mathrm{in}} \\
&\quad\to \tfrac{1}{4}\big(b_1^{\dagger 2}+b_2^{\dagger 2}-b_3^{\dagger 2}-b_4^{\dagger 2}-2b_1^\dagger b_2^\dagger+2b_3^\dagger b_4^\dagger\big)|0000\rangle_{\mathrm{out}} \\
&a_3^\dagger a_4^\dagger|0000\rangle_{\mathrm{in}} \\
&\quad\to \tfrac{1}{4}\big(b_1^{\dagger 2}-b_2^{\dagger 2}+b_3^{\dagger 2}-b_4^{\dagger 2}-2b_1^\dagger b_3^\dagger+2b_2^\dagger b_4^\dagger\big)|0000\rangle_{\mathrm{out}}.
\end{aligned}
\tag{9}
$$

Here, we ignore the case in which two or more photons come from one user, or two or more photons are detected at one detector. Then, using Eq. (9), we derive states $|\Phi\rangle_{X_1\ldots X_4}$ of the remaining subsystems depending on the detection pattern. Table I lists the detection pattern (the detectors clicked) and the resulting states at the end users.

Suppose detectors 1 and 2 detect single photons. If we denote the entire state after the transmission and interference $|\Psi'\rangle$, the state in subsystem $X_1 \ldots X_4$ becomes

$$
\begin{aligned}
|\Phi\rangle\langle\Phi|_X &= \mathrm{Tr}_{X'}[\langle 1100|_{X'}(|\Psi'\rangle\langle\Psi'|_{XX'})|1100\rangle_{X'}] \\
&= \tfrac{1}{2}(|1010\rangle-|0101\rangle)(\langle 1010|-\langle 0101|),
\end{aligned}
\tag{10}
$$

where we use a simplified notation $X_1 \ldots X_4 \to X$ and $X_1' \ldots X_4 \to X'$. Note that the circuit in Fig. 2(a) was also used in [33,35] to generate (or project to) W and Dicke states and is analyzed also in the context of linear optical quantum computing without considering losses [36].

B. Generalization of the central node

For simplicity, we assume that N is even. The Appendix discusses the case with odd N. To generate GHZ states with $N > 4$, we use a circuit from Fig. 2(a) as a building block. However, to obtain larger GHZ states, this circuit is not extended trivially. For that, we propose to use a setup as in Fig. 2(c). Here, copies of circuit Fig. 2(a) are connected through the edge modes by means of auxiliary circuits with a single photon source as in Fig. 2(b). This method succeeds if one of the following detection patterns (1, 2), (1, 3), (1, 4), (2, 3), (2, 4), (3, 4) is signalized in each of the building block circuits. Thus, in the circuit in Fig. 2(c), we have 36 four-photon detection patterns that, up to known local unitaries, leading to $|\mathrm{GHZ}\rangle_6$ in six user nodes. By analogously connecting more four-mode circuits with adjacent

TABLE I. States in subsystem $X_1 \ldots X_4$ depending on detection pattern in subsystem $X_1' \ldots X_4'$.

Detection pattern	State $\|\Phi\rangle_{X_1\ldots X_4}$
1,2	$\frac{1}{\sqrt{2}}(\|1010\rangle-\|0101\rangle)$
1,3	$\frac{1}{\sqrt{2}}(\|1100\rangle-\|0011\rangle)$
1,4	$\frac{1}{\sqrt{2}}(\|1001\rangle-\|0110\rangle)$
2,3	$\frac{1}{\sqrt{2}}(-\|1001\rangle+\|0110\rangle)$
2,4	$\frac{1}{\sqrt{2}}(-\|1100\rangle+\|0011\rangle)$
3,4	$\frac{1}{\sqrt{2}}(-\|1010\rangle+\|0101\rangle)$

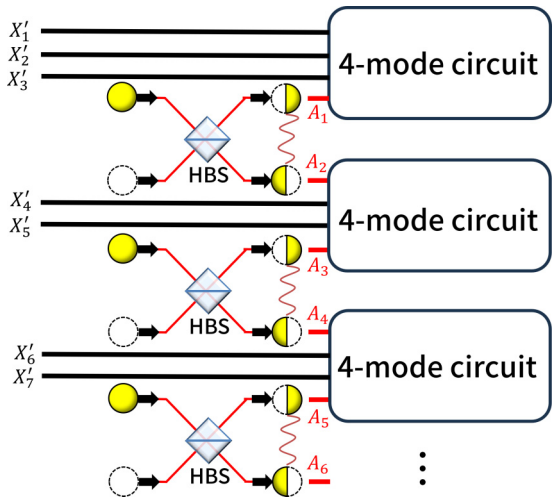

FIG. 3. Loss-tolerant GHZ distribution protocol for N users. HBS: half beam splitter.

auxiliary modes, the circuit can be expanded to generate $|\mathrm{GHZ}\rangle_N$ with arbitrary N (see Fig. 3).

The required resource budget consists of $\frac{N}{2}-1$ four-mode building blocks, $N-4$ auxiliary modes, $2N-4$ detectors, and $\frac{N}{2}-1$ single-photon sources.

C. Performance analysis under the ideal condition

In this subsection, we analyze the performance of our protocol. Here, we consider only losses; other imperfections will be discussed in the next section. To consider loss in each channel, we introduce ancillary modes E_i for each subsystem X_i' and describe photon loss as the interaction between mode X_i' and E_i via a beam splitter.

$$|1\rangle_{X_i'}|0\rangle_{E_i} \to \sqrt{\eta}|1\rangle_{X_i'}|0\rangle_{E_i} + \sqrt{1-\eta}|0\rangle_{X_i'}|1\rangle_{E_i}. \tag{11}$$

Denote this beam-splitting unitary as U_{loss}. Since E_i is uncontrollable, we describe the evolution of subsystem X_i' by averaging over the degrees of freedom of E_i as follows:

$$\mathrm{Tr}_{E_i}(U_{\mathrm{loss}}|\psi\rangle\langle\psi|X_i' \otimes |0\rangle\langle 0|E_i U_{\mathrm{loss}}^\dagger). \tag{12}$$

The transmittance of the beam splitter and the channel are assumed to be equal to the link power transmittance η. For any even N due to the symmetry of channel loss and the circuit, the success probability is always the same for all possible successful detection patterns. Therefore, without loss of generality, hereafter we consider a particular detection pattern that the first and second detectors in each four-mode building block detect single photons. This means that the state at the detectors are projected onto $|1100\ldots1100\rangle_{X'A}$, where A indicates auxiliary modes. Consider the initial state, before the channel transmission but including the auxiliary modes, represented by a superposition in the photon number basis. The terms that have finite probability to be projected onto $|1100\ldots1100\rangle_{X'A}$ are in the form of $|\psi\rangle_X|1i_1 1i_2 1i_3\ldots 1i_{N-2}\rangle_{X'A}$ and $|\psi\rangle_X|j_1 1 j_2 1 j_3 1\ldots j_{N-2}1\rangle_{X'A}$, where $i_l, j_l = 0, 1\ \forall l$. $|\psi\rangle$ are some states depending on $\{i_l\}_l$ and $\{j_l\}_l$. In the superposition form, the probability amplitudes of these terms are

$$Y_m = a^{\frac{N}{2}-m} b^{\frac{N}{2}+m} \times \left(\frac{1}{\sqrt{2}}\right)^{\frac{N}{2}-2}, \tag{13}$$

where $m = 0, 1, 2, \ldots, N/2$ is the number of modes in which i_l or j_l are 1. After the successive detection event, i.e., transmission and projection onto $|1100\ldots1100\rangle_{X'A}$, the initial state reads

$$\rho_X = \frac{1}{\sqrt{\mathcal{N}}}\left(p_0 Y_0^2 |\Phi\rangle\langle\Phi| \sum_{m=1}^{\frac{N}{2}} p_m Y_m^2 \sum_{k}^{2\binom{N/2}{m}} |\phi_{mk}\rangle\langle\phi_{mk}|\right), \tag{14}$$

where $|\Phi\rangle$ is the desired GHZ state, $|\phi_{mk}\rangle$ are some states that are orthogonal to $|\Phi\rangle$, and $\mathcal{N}$ is a normalization factor. Physically, m is the number of photons that are lost during the transmission and $|\phi_{mk}\rangle$ is an unwanted state that are lost m photons during the channel transmission and is projected onto $|1100\ldots1100\rangle_{X'A}$ with nonzero probability. For each m, there are $2 \times {}^{N/2}C_m$ different $|\phi_{mk}\rangle$, where 2 comes from two types of the terms, $|1i_1 1i_2\ldots\rangle_{X'A}$ and $|j_1 1 j_2 1\ldots\rangle_{X'A}$, and each of them has ${}^{N/2}C_m$ combinations of $\{i_l\}_l$ and $\{j_l\}_l$. Thus, k is just the index of the states. p_m is the probability that the subsystem of $X'A$ with m photon loss are projected onto $|1100\ldots1100\rangle_{X'A}$. They are given by

$$p_m = \eta^{\frac{N}{2}}(1-\eta)^m \times \left(\tfrac{1}{4}\right)^{\frac{N}{2}-1}, \tag{15}$$

and combining it with Eq. (13), we have

$$\begin{aligned} p_m Y_m^2 &= \eta^{\frac{N}{2}}(1-\eta)^m \times \left(\tfrac{1}{4}\right)^{\frac{N}{2}-1} \times a^{N-2m} b^{N+2m} \times \left(\tfrac{1}{2}\right)^{\frac{N}{2}-2} \\ &= \eta^{\frac{N}{2}}(1-\eta)^m \left(\tfrac{1}{2}\right)^{\frac{3}{2}N-4} a^{N-2m} b^{N+2m}. \end{aligned} \tag{16}$$

Then, we have the probability of obtaining the target detection pattern as

$$\begin{aligned} P &= 2\sum_{m=0}^{\frac{N}{2}} p_m Y_m^2 \times {}^{\frac{N}{2}}C_m \\ &= 2\sum_{m=0}^{\frac{N}{2}} \eta^{\frac{N}{2}}(1-\eta)^m \left(\frac{1}{2}\right)^{\frac{3}{2}N-4} a^{N-2m} b^{N+2m} \times {}^{\frac{N}{2}}C_m \\ &= \left(\frac{1}{2}\right)^{\frac{3}{2}N-5} \eta^{\frac{N}{2}} b^N \sum_{m=0}^{\frac{N}{2}} {}^{\frac{N}{2}}C_m (a^2)^{\frac{N}{2}-m} (b^2(1-\eta))^m \\ &= \left(\frac{1}{2}\right)^{\frac{3}{2}N-5} \eta^{\frac{N}{2}} b^N [a^2 + b^2(1-\eta)]^{\frac{N}{2}}. \end{aligned} \tag{17}$$

The total distribution rate R is obtained by multiplying P by the number of combinations of detection patterns which lead to the GHZ states, i.e.,

$$R = 6^{\frac{N}{2}-1} \times P = 3^{\frac{N}{2}-1}\left(\tfrac{1}{2}\right)^{N-4} \eta^{\frac{N}{2}} b^N [a^2 + b^2(1-\eta)]^{\frac{N}{2}}, \tag{18}$$

where we note that 6 is the number of the detection patterns at each four-mode building block and $N/2-1$ is the number of the building blocks.

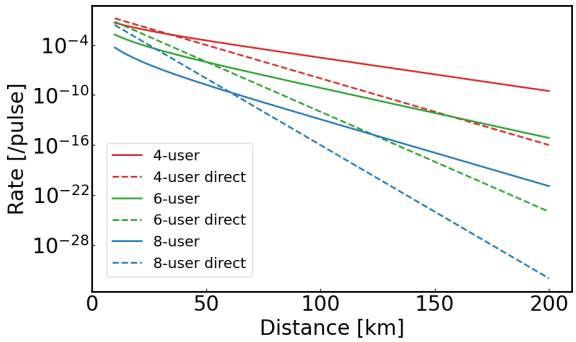

FIG. 4. GHZ generation rate versus distance for different numbers of users. The fidelity is fixed at 0.9. The top-red, middle-blue, and bottom-green lines, respectively, represent cases of four, six, and eight users. The solid lines indicate our protocol, while the dashed lines show the direct transmission, the rate of which is η^N. The lines characterizing the scenario with more users show a lower rate.

The fidelity between ρ_X and the ideal GHZ state is also derived as

$$F = \sqrt{\langle\Phi|\rho_X|\Phi\rangle} = \sqrt{\frac{4Y_0^2 p_0}{2P}} = \sqrt{\frac{a^N}{[a^2 + b^2(1-\eta)]^{\frac{N}{2}}}}. \quad (19)$$

Figure 4 shows the distribution rates R from Eq. (18) of this protocol and the direct transmission protocol for $N = 4, 6, 8$ user nodes. Here, we assume that the rate of the direct transmission is

$$R_{\text{direct}} \equiv \eta^N. \quad (20)$$

Figure 5 shows the dependence of the rate on the distance for fixed fidelities and comparison with the performance of the direct transmission protocol. In both figures, the fiber loss is assumed to be typical, 0.2 (dB/km). The figures confirm the advantage of the proposed protocol with respect to the direct transmission method, especially in the limit of large distances with larger loss and when the number of users increases.

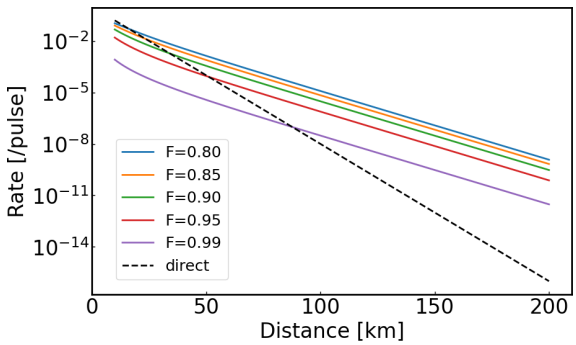

FIG. 5. GHZ generation rate versus distance for different fidelities. The fidelity varies between 0.8 and 0.99. The number of user nodes is four. The solid lines indicate our protocol, while the dashed line is the direct transmission. The lines with lower rate are characterized by the higher fidelity.

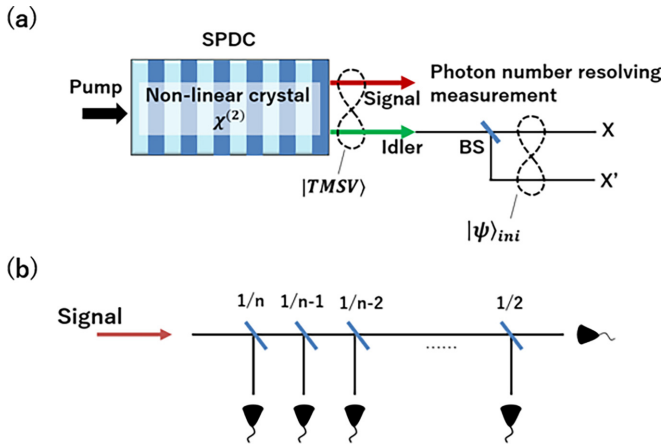

FIG. 6. (a) Schematic image of the SPDC source. The signal mode is input to the photon number-resolving system (PNRD). The idler mode is split by a beamsplitter (BS) into mode X and X'. (b) An example of the setup performing quasi-PNRD with threshold detectors. The numbers above each beamsplitter indicate respective reflectance. The click in only one detector indicates a quasi-single-photon state in the idler mode which is the input in our protocol.

III. IMPLEMENTATION WITH SPDC SOURCES

A. Scheme

In realistic experimental setups one could use the input states Eq. (4) ideally generated with single-photon sources such as trapped ions [37,38], NV centers [39], or quantum dots [40]. However, these solutions require advanced technology which we want to avoid, instead here, we propose to use another source of quantum states approximating Eq. (4): an optical system with spontaneous parametric down conversion (SPDC). It is feasible with the current technology and widely used in quantum optics experiments. Such a source generates the two-mode squeezed vacuum (TMSV) state in the signal and idler modes, S and I,

$$|\text{TMSV}\rangle = \sqrt{1-\lambda^2}\sum_{n=0}^{\infty}\lambda^n|n\rangle_S|n\rangle_I. \quad (21)$$

Here, $|n\rangle$ indicates the n-photon number state, $\lambda = \tanh r$, and r is the squeezing parameter. We refer to the squeezing level in dB as $20\log_{10}e^r(\text{dB})$. The multiphoton terms in TMSV cause reduction of fidelity since we cannot distinguish if two photons come from the same or different sources. To avoid this, we use the heralded single photon by measuring the photon number of the signal mode. The initial state is prepared by splitting the signal by an asymmetric beam splitter

$$|\psi\rangle_{\text{ini}} = \sqrt{t}|10\rangle_{X_i X_i'} + \sqrt{1-t}|01\rangle_{X_i X_i'}, \quad (22)$$

where t is the transmittance of the beam splitter (BS) in Fig. 6(a).

While the technology of PNRDs developing, one can also realize a quasi-PNRD by multiplexing threshold detectors, which discriminate only zero or nonzero photons. An example of that is illustrated in Fig. 6(b). It allows us to decrease the probability of wrongly counting the photon number. Indeed, in case of the two-photon term, the probability that one detector detects two photons in the signal mode is $1/n$, where n is the

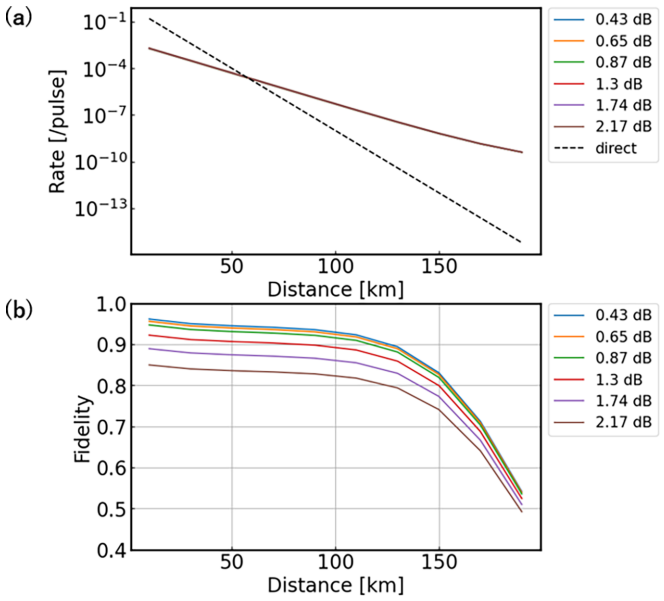

FIG. 7. (a) GHZ generation rate versus distance for different squeezing levels. The solid lines indicate our protocol, while the dashed line shows the direct transmission. (b) Fidelity versus distance for different squeezing levels. The lines with smaller fidelity are characterized by larger squeezing.

number of detectors. More generally, if k photons are input to this system, the probability that we mistakenly recognize the state as the single-photon state is $(1/n)^{k-1}$. By increasing n, one can identify the single-photon state in the idler mode with arbitrary precision.

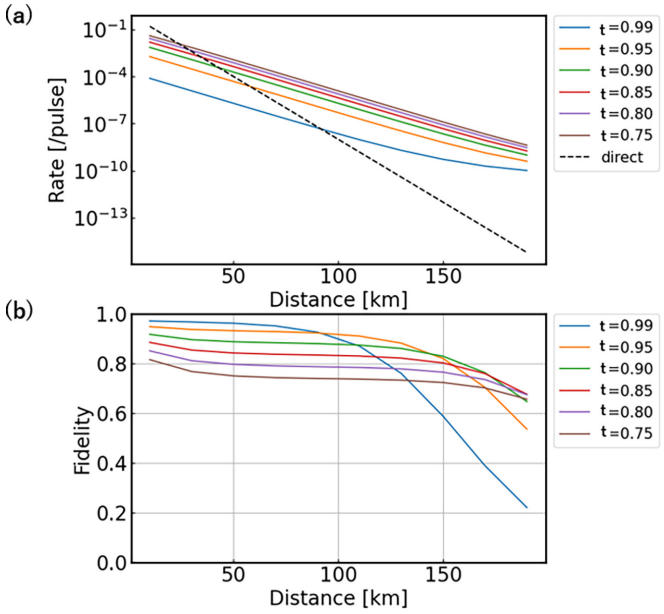

FIG. 8. (a) GHZ generation rate versus distance for different values of t in (22). The lower rate lines are characterized by larger t. (b) Fidelity versus distance for different values of t. The solid lines indicate our protocol, while the dashed line indicates the direct transmission. The lines with higher fidelity for short distances are characterized by larger t.

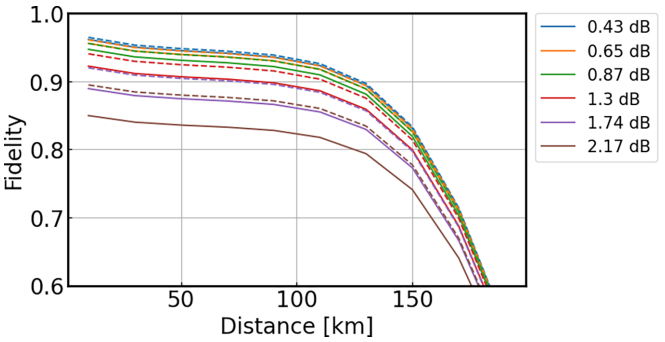

FIG. 9. Fidelity versus distance for different levels of squeezing. The solid lines are generated using quasi-PNRD with three detectors, while the dashed lines indicate perfect PNRD. The lines showing lower fidelities are characterized by higher squeezing. Here, $t = 0.95$.

B. Rate and fidelity under realistic conditions

We assume detector efficiency of 80% with dark count rate of 10^{-6}, which are conservative numbers, as better detectors, both in terms of efficiency and the dark count rate, are currently available [41–43]. The rate and fidelity under these conditions can be calculated by using Gaussian states formalism [44–46] with a PYTHON library "THEWALRUS" [47]. In this analysis, one attempt means that all users send their subsystems X' to the central node. Figure 7 shows the GHZ states' generation rates and the fidelities of the states for different squeezing levels in the four-users case. We fix t in Eq. (22) at 0.95. Figure 7(a) suggests that the distribution rate is independent of the squeezing in TMSV. However, this only reflects the fact that we do not include the input state generation process into the rate. However, the fidelity strongly depends on the squeezing level. This means that the multi-photon residues in the initial states is an important factor of the fidelity reduction. Figure 8 shows the generation rates and fidelities for different values of transmittance t in Eq. (22). This figure shows the trade-off between the rate and fidelity. We observe that at some distance the dark counts dominate the detection. Then the generation rate tends to a constant value, however, the fidelity drops down abruptly.

To see the effect of PNRD accuracy on the fidelity, we compare the PNRD and the quasi-PNRD with three threshold detectors. The result is in Fig. 9, where we fix t at 0.95. The dashed lines indicate the PNRD and the solid lines are for the quasi-PNRD with three detectors. We observe that the fidelities are almost the same for these two cases, especially in the small squeezing regime. This is because the smaller the squeezing, the smaller the probability of getting two or more photon terms in the signal and idler modes.

Figure 10 shows the optimized generation rate for different values of fidelity. We fix the squeezing level at 0.43 dB and optimize the other parameters to obtain the highest rate satisfying the fidelity condition. We also assume perfect PNRD since the gap compared to quasi-PNRD is very small in 0.43 dB squeezing parameter (see Fig. 12). The rate at the limiting distance of the protocol approximately coincides with the assumed rate of detectors' dark counts and can be improved by improving the detectors' quality. Also, here, we observe a trade-off between the rate and fidelity, as the rate of higher

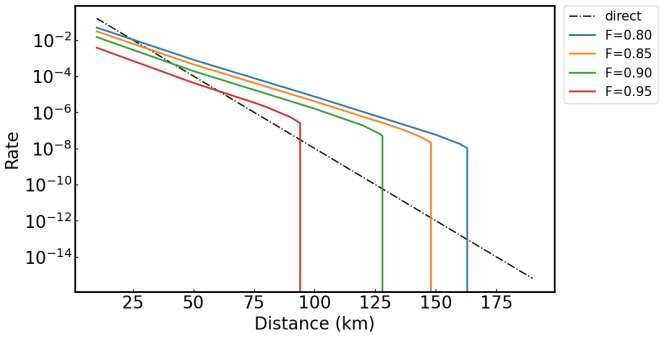

FIG. 10. GHZ generation rate versus distance for different values of the fidelity. Solid lines indicate our protocol and dashed line the direct transmission. The line with the lowest rate is characterized by the highest fidelity.

fidelity states is lower. The figure shows the advantage of our protocol even with feasible photon sources and realistic and conservative experimental parameters.

IV. APPLICATION TO THE DISTRIBUTED SURFACE CODE

In this section, we briefly discuss a possible application of our protocol in a distributed architecture for topological quantum computing with noisy network channels proposed in [48]. There, many simple processor cells with a few qubits each are networked via noisy links as shown in Fig. 11. In this scheme, each data qubit is placed in a different network cell. The main difference with respect to the standard surface codes is that instead of using adjacent auxiliary qubits for the stabilizer measurements, four-partite GHZ states are distributed to neighboring four cells to perform the stabilizer measurements among them. In consequence, the main challenge for such an architecture is the ability to distribute high-quality GHZ states at a high rate.

To address the GHZ distribution problem, the solution proposed in [49] includes two steps: first, distribute high-quality bipartite states with an efficient photonic linking protocol, called the "extreme photon loss" (EPL) protocol [50]; and second, fuse and purify the bipartite entanglement to create high-quality GHZ states. With long-enough coherence times [51], this combination has noise thresholds comparable with

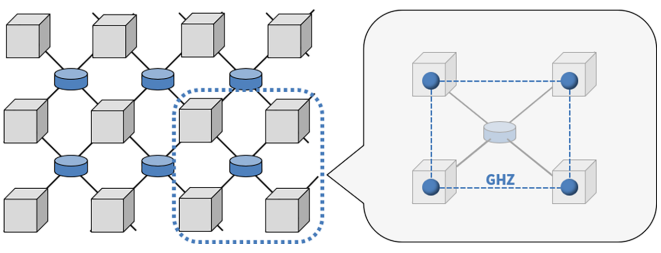

FIG. 11. Scheme of distributed 2D surface code architecture. Gray boxes are the cells consisting of a small number of qubits. Blue cylinders are the central nodes connected via fibers (black lines) to four nearby cells. The nearest four cells share a GHZ state, which plays the same roll as the stabilizer in the surface code.

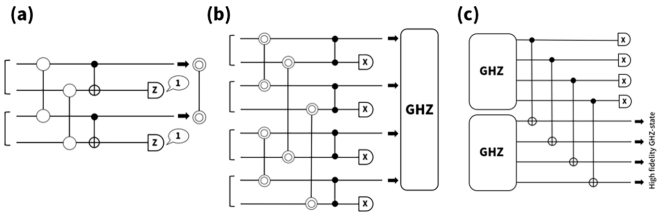

FIG. 12. (a) Bell states' purification of the EPL protocol. (b) GHZ-state distillation. (c) Purification process to get higher fidelity GHZ states as in [49].

monolithic architectures even in the presence of link losses and noise.

The generation of distributed surface code in a two-dimensional (2D) regular quadrilateral grid of memory cells, as discussed in the original proposal [49], is schematically shown in Fig. 12. The first stage of that protocol consists in distribution and purification of the Bell states between neighboring nodes [Fig. 12(a)]. Purification was proposed to be performed according to the extreme photon loss (EPL) protocol [50]. Then the GHZ states are distilled as shown in Fig. 12(b) and purified Fig. 12(c).

Here, we generalize the bipartite purification in the EPL protocol to more than two end users (see Fig. 13) showcasing the feasibility of our protocol to prepare high-quality GHZ states. In consequence, our protocol can replace the two-step process of bipartite entanglement generation and GHZ purification. A drawback of fusing bipartite entanglement is that, even in the absence of further purification, two-qubit gates are needed, severely impacting performance [51]. Our protocol allows for a direct generation of the GHZ state among the four neighboring cells, sidestepping the need of two-qubit gates for fusion. Quantitative evaluation of this advantage requires intense numerical simulations and deserves separate research.

Here we discuss the details of the procedure of GHZ-state purification from the mixed state

$$\rho = \alpha|\Phi\rangle\langle\Phi| \sum \beta_i|\phi_i\rangle\langle\phi_i|, \tag{23}$$

where $\alpha + \sum \beta_i = 1$ and $\{|\phi_i\rangle\}$ are undesirable states. We notice that different configurations of detectors signalize mixed GHZ states up to different local unitary transformations. The local transformations can correct the first component of the

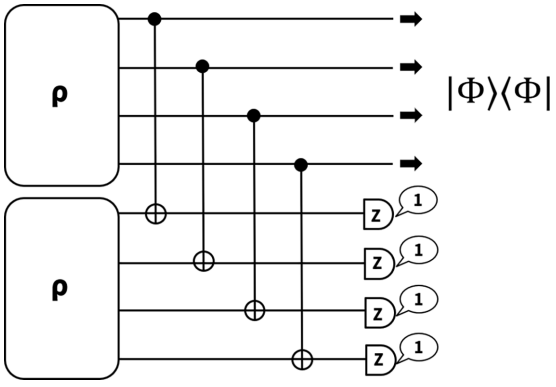

FIG. 13. GHZ-state purification of our protocol.

T \ C	1010	0101	1100	0011	1001	0110	1110	1101	1011	0111	1111
1010	0000	1111	0110	1001	0011	1001	0100	0111	0001	1101	0101
0101	1111	0000	1001	0110	1100	0011	1011	1000	1110	0010	1010
1100	0110	1001	0000	1111	0101	1010	0010	0001	0111	1011	0011
0011	1001	0110	1111	0000	1010	0101	1101	1110	1000	0100	1100
1001	0011	1100	0101	1010	0000	1111	0111	0100	0010	1110	0110
0110	1001	1011	1010	0101	1111	0000	1000	1011	1101	0001	1001
1110	0100	1000	0010	1101	0111	1000	0000	0011	0101	1001	0001
1101	0111	1110	0001	1110	0100	1011	0011	0000	0110	1010	0010
1011	0001	1010	0111	1000	0010	1101	0101	0110	0000	1100	0100
0111	1101	0010	1011	0100	1110	0001	1001	1010	1100	0000	1000
1111	0101	1010	0011	1100	0110	1001	0001	0010	0100	1000	0000

FIG. 14. The first row and column of the table show the terms from two copies of the mixed state (23), respectively. Here the first copy serves as the control system (C), while the second as the target (T). The inner part of the table shows values of the target states' terms after a set of CNOT. Table of the state to which target states transform through CNOT operation. "C" means control qubits and "T" means target qubits. If we get the results in green part, the unwanted terms could be in the control qubits. The measurement 1111 is the only result which heralds the elimination of unwanted terms denoted in the last columns and rows (in green), and hence, the success of the GHZ-state purification. We distinguished pairs of states that correspond to the same set of detectors generating the mixed states in our protocol.

Eq. (23), but the undesirable contributions are not transformed to the same set. Therefore, the purification procedure requires observing a given patterns of detection events which reduces the rate by a constant factor. Let us explain how to generalize the EPL protocol. As we mentioned, the appropriate patterns of photon detections in the central node signal the generation of a mixed state Eq. (23) in our protocol.

In particular, if detectors 1 and 2 in the central node simultaneously click, the ideal term $|\Phi\rangle$ is $|\Phi\rangle = (|1010\rangle - |0101\rangle)/\sqrt{2}$ and the unwanted terms $|\phi_i\rangle \in \{|1011\rangle, |1110\rangle, |0111\rangle, |1101\rangle, |1111\rangle\}$. We assume that we have two copies of ρ with the same ideal $|\Phi\rangle$ from (23) and perform purification just like the Bell-state purification in the EPL protocol: in the qubit basis, each cell locally applies CNOT operation to the part of ρ and measures the target qubits in the Z basis. As can be seen from $|\Phi\rangle$ and $\{|\phi\rangle\}$, there is no pair to transform the target qubits into $|1111\rangle$ other than {control:$|0101\rangle$, target:$|1010\rangle$} and vice versa (see Fig. 14).

Thus, like the EPL protocol, we can eliminate the unwanted terms by selecting the cases with measurement results "1" in all cells. The probability of obtaining this result is $P = 0.5\alpha \leqslant 0.5$. The higher α, the higher the success probability of purification. However, to obtain high α, the probability that a cell emits a photon must be small which implies longer time to distribute one ρ. So, to get the highest distribution rate including the purification process, one needs to optimize over the coefficients of the initial state.

Concluding, we propose to simplify the original protocol [49] by replacing the process of Bell-state generation, purification, and the GHZ-state distillation by our direct GHZ generation protocol and distillation by the procedure described above.

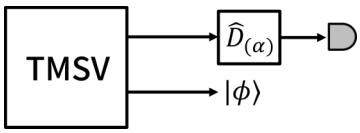

FIG. 15. Displacement on one of the two modes and projective measurement to $|1\rangle$ (photon number resolving detection).

V. CONCLUSION

In this paper, we propose a practical, loss-tolerant protocol that directly generates GHZ states in a lossy star network with realistic experimental conditions. The protocol beats the rate of the direct transmission protocol and shifts the common paradigm in which the multipartite entangled states are distilled from bipartite Bell states. We give rigorous formulas for the generation rate and fidelity assuming locally produced Bell states or TMSV as the input to the protocol. The main factors that degrade the fidelity are multiple photons in the source, channel loss, and detectors' dark counts. Our protocol can directly impact the known GHZ-based protocols such as the conference key agreement or distributed quantum sensing. Moreover, we propose its application for distributed codes in quantum computing. Among future research direction we can indicate the investigation of the effect of phase noise in the transmission process like in [52]. Moreover, the paper paves the way to design alternative protocols of distribution of general multipartite entanglement states in quantum networks.

ACKNOWLEDGMENTS

We thank Daniel Bhatti for helpful comments on an earlier version of this paper. This work was supported by JST Moonshot R&D Grants No. JPMJMS226C, No. JPMJMS2061, No JST COI-NEXT, and No. JPMJPF2221, and Program for the Advancement of Next Generation Research Projects, Keio University.

APPENDIX: IN THE CASE THAT THE NUMBER OF USER NODES IS ODD

Let us also clarify the procedure in the case when the number of user nodes is odd, i.e., $2k-1$ ($k \in N$). Then, one should use the optical circuit for $2k$ user nodes and input states

$$\frac{|0\rangle + \alpha|1\rangle}{1+|\alpha|^2}, \tag{A1}$$

into the modes that are not used. As a source of this state, we propose a setup with a two-mode squeezed vacuum source, displacement, and photon number-resolving detection. Here, α must be fixed equal to the probability of a photon entering other modes. Then the distribution rate is estimated as $O(\eta^k)$, which shows the same advantage of the protocol over the direct transmission.

We describe the details to generate the state Eq. (A1) below. The scheme is shown in Fig. 15. Assume two mode-squeezed vacuum states

$$|\mathrm{TMSV}\rangle_{SI} = \sqrt{1-\lambda^2}\sum_{n=0}\lambda^n |n\rangle_S |n\rangle_I. \tag{A2}$$

According to the authors of [53], the coefficients of the displacement operator are

$$\langle n|\hat{D}_{(\alpha)}|m\rangle = \sqrt{\frac{m!}{n!}}\alpha^{n-m}e^{-|\alpha|^2/2}L_m^{n-m}(|\alpha|^2) \ \ (n \geqslant m),$$
$$\langle n|\hat{D}_{(\alpha)}|m\rangle = \sqrt{\frac{n!}{m!}}\alpha^{m-n}e^{-|\alpha|^2/2}L_n^{m-n}(|\alpha|^2) \ \ (n \leqslant m), \quad \text{(A3)}$$

where $L_n^{(l)}(x)$ is the associated Laguerre polynomial defined by

$$L_n^{(l)}(x) = \sum_{k=0}\binom{n+l}{n-k}\frac{(-x)^k}{k!}. \quad \text{(A4)}$$

After the displacement operation, we perform the projective measurement of $|1\rangle$ in the signal mode. So, the relevant terms of displacement operator are $|1\rangle\langle n|$, as follows:

$$\alpha e^{-|\alpha|^2/2}|1\rangle\langle 0|,$$
$$e^{-|\alpha|^2/2}(1-|\alpha|^2)|1\rangle\langle 1|,$$
$$\sqrt{\frac{1}{2}}\alpha e^{-|\alpha|^2/2}(2-|\alpha|^2)|1\rangle\langle 2|,$$
$$\sqrt{\frac{1}{6}}\alpha^2 e^{-|\alpha|^2/2}(3-|\alpha|^2)|1\rangle\langle 3|,$$
$$\sqrt{\frac{1}{24}}\alpha^3 e^{-|\alpha|^2/2}(4-|\alpha|^2)|1\rangle\langle 4|, \ldots. \quad \text{(A5)}$$

Thus, the state $|\phi\rangle$ in the idler mode is

$$|\phi\rangle_I = {}_S\langle 1|\hat{D}_{(\alpha)}|\text{TMSV}\rangle_{SI}$$
$$= \frac{1}{\sqrt{\mathcal{N}}}\left\{\alpha|0\rangle_I+\lambda(1-|\alpha|^2)|1\rangle_I+\sqrt{\frac{1}{2}}\alpha\lambda^2(2-|\alpha|^2)|2\rangle_I\right.$$
$$\left.+\sqrt{\frac{1}{6}}\alpha^2\lambda^3(3-|\alpha|^2)|3\rangle_I+\cdots\right\}. \quad \text{(A6)}$$

If $\lambda^2 \ll |\alpha|^2 \ll 1$, the probability of two photons coming from the input state is

$$P_{\text{noise}} = \frac{1}{2\mathcal{N}}|\alpha|^2\lambda^4(2-|\alpha|^2)^2 \approx \frac{2|\alpha|^2\lambda^4}{|\alpha|^2} = 2\lambda^4, \quad \text{(A7)}$$

and the probability of two photons entering from two different modes is

$$P_{\text{target}} = \frac{\lambda^2(1-|\alpha|^2)}{\mathcal{N}} \times \frac{\lambda^2(1-|\alpha|^2)}{\mathcal{N}} \approx \frac{\lambda^4}{|\alpha|^4}, \quad \text{(A8)}$$

where $\mathcal{N} \approx |\alpha|^2$. Since $P_{\text{noise}} \ll P_{\text{target}}$, we can use $|\phi\rangle$ as the ancillary input state with an odd number of users.

[1] S. Wehner, D. Elkouss, and R. Hanson, Quantum internet: A vision for the road ahead, Science **362**, eaam9288 (2018).

[2] H. J. Kimble, The quantum internet, Nature (London) **453**, 1023 (2008).

[3] N. Gisin and R. Thew, Quantum communication, Nat. Photon. **1**, 165 (2007).

[4] C. H. Bennett and G. Brassard, Quantum cryptography: Public key distribution and coin tossing, Theor. Comput. Sci. **560**, 7 (2014).

[5] A. K. Ekert, Quantum cryptography based on Bell's theorem, Phys. Rev. Lett. **67**, 661 (1991).

[6] C. H. Bennett, G. Brassard, and N. D. Mermin, Quantum cryptofraphy without Bell's theorem, Phys. Rev. Lett. **68**, 557 (1992).

[7] M. Proietti, J. Ho, F. Grasselli, P. Barrow, M. Malik, and A. Fedrizzi, Experimental quantum conference key agreement, Sci. Adv. **7**, eabe0395 (2021).

[8] G. Carrara, G. Murta, and F. Grasselli, Overcoming fundamental bounds on quantum conference key agreement, Phys. Rev. Appl. **19**, 064017 (2023).

[9] P. Kómár, E. M. Kessler, M. Bishof, L. Jiang, A. S. Sørensen, J. Ye, and M. D. Lukin, A quantum network of clocks, Nat. Phys. **10**, 582 (2014).

[10] D. Gottesman, T. Jennewein, and S. Croke, Longer-baseline telescopes using quantum repeaters, Phys. Rev. Lett. **109**, 070503 (2012).

[11] E. T. Khabiboulline, J. Borregaard, K. De Greve, and M. D. Lukin, Quantum-assisted telescope arrays, Phys. Rev. A **100**, 022316 (2019).

[12] Z. Eldredge, M. Foss-Feig, J. A. Gross, S. L. Rolston, and A. V. Gorshkov, Optimal and secure measurement protocols for quantum sensor networks, Phys. Rev. A **97**, 042337 (2018).

[13] W. Ge, K. Jacobs, Z. Eldredge, A. V. Gorshkov, and M. Foss-Feig, Distributed quantum metrology with linear networks and separable inputs, Phys. Rev. Lett. **121**, 043604 (2018).

[14] K. Qian, Z. Eldredge, W. Ge, G. Pagano, M. Foss-Feig, C. Monroe, J. V. Porto, and A. V. Gorshkov, Heisenberg-scaling measurement protocol for analytic functions with quantum sensor networks, Phys. Rev. A **100**, 042304 (2019).

[15] T. Qian, J. Bringewatt, I. Boettcher, P. Bienias, and A. V. Gorshkov, Optimal measurement of field properties with quantum sensor networks, Phys. Rev. A **103**, L030601 (2021).

[16] A. S. Cacciapuoti, M. Caleffi, F. Tafuri, F. S. Cataliotti, S. Gherardini, and G. Bianchi, Quantum internet: Networking challenges in distributed quantum computing, IEEE Network **34**, 137 (2020).

[17] R. Van Meter and S. J. Devitt, The path to scalable distributed quantum computing, Computer **49**, 31 (2016).

[18] C. H. Bennett, G. Brassard, C. Crepeau, R. Jozsa, A. Peres, and W. K. Wootters, Teleporting an unknown quantum state via dual classical and Einstein-Podolsky-Rosen channels, Phys. Rev. Lett. **70**, 1895 (1993).

[19] M. Epping, H. Kampermann, C. Macchiavello, and D. Bruß, Multi-partite entanglement can speed up quantum key distribution in networks, New J. Phys. **19**, 093012 (2017).

[20] H. Yamasaki, A. Pirker, M. Murao, W. Dür, and B. Kraus, Multipartite entanglement outperforming bipartite entanglement

under limited quantum system sizes, Phys. Rev. A **98**, 052313 (2018).
[21] M. Takeoka, S. Guha, and M. M. Wilde, Fundamental rate-loss tradeoff for optical quantum key distribution, Nat. Commun. **5**, 5235 (2014).
[22] S. Pirandola, R. Laurenza, C. Ottaviani, and L. Banchi, Fundamental limits of repeaterless quantum communications, Nat. Commun. **8**, 15043 (2017).
[23] H. J. Briegel, W. Dür, J. I. Cirac, and P. Zoller, Quantum repeaters: The role of imperfect local operations in quantum communication, Phys. Rev. Lett. **81**, 5932 (1998).
[24] L.-M. Duan, M. D. Lukin, J. I. Cirac, and P. Zoller, Long-distance quantum communication with atomic ensembles and linear optics, Nature (London) **414**, 413 (2001).
[25] N. Sangouard, C. Simon, H. de Riedmatten, and N. Gisin, Quantum repeaters based on atomic ensembles and linear optics, Rev. Mod. Phys. **83**, 33 (2011).
[26] W. J. Munro, K. Azuma, K. Tamaki, and K. Nemoto, Inside quantum repeaters, IEEE J. Sel. Top. Quantum Electron. **21**, 78 (2015).
[27] K. Azuma, S. Bäuml, T. Coopmans, D. Elkouss, and B. Li, Tools for quantum network design, AVS Quantum Sci. **3**, 014101 (2021).
[28] K. Azuma, S. E. Economou, D. Elkouss, P. Hilaire, L. Jiang, H.-K. Lo, and I. Tzitrin, Quantum repeaters: From quantum networks to the quantum internet, Rev. Mod. Phys. **95**, 045006 (2023).
[29] G. Avis, F. Rozpędek, and S. Wehner, Analysis of multipartite entanglement distribution using a central quantum-network node, Phys. Rev. A **107**, 012609 (2023).
[30] Y. Hasegawa, R. Ikuta, N. Matsuda, K. Tamaki, H. K. Lo, T. Yamamoto, K. Azuma, and N. Imoto, Experimental time-reversed adaptive Bell measurement towards all-photonic quantum repeaters, Nat. Commun. **10**, 378 (2019).
[31] V. Krutyanskiy, M. Canteri, M. Meraner, J. Bate, V. Krcmarsky, J. Schupp, N. Sangouard, and B. P. Lanyon, Telecom-wavelength quantum repeater node based on a trapped-ion processor, Phys. Rev. Lett. **130**, 213601 (2023).
[32] A. J. Stolk *et al.*, Metropolitan-scale heralded entanglement of solid-state qubits, Sci. Adv. **10**, eadp6442 (2024).
[33] W. Roga, R. Ikuta, T. Horikiri, and M. Takeoka, Efficient Dicke state generation in a network of lossy channels, Phys. Rev. A **108**, 012612 (2023).
[34] M. J. Bayerbach, S. E. D'Aurelio, P. van Loock, and S. Barz, Bell-state measurement exceeding 50% success probability with linear optics, Sci. Adv. **9**, eadf4080 (2023).
[35] P. Lougovski, S. J. van Enk, K. S. Choi, S. B. Papp, H. Deng, and H. J. Kimble, Verifying multipartite mode entanglement of W states, New J. Phys. **11**, 063029 (2009).
[36] S. Bartolucci, P. M. Birchall, M. Gimeno-Segovia, E. Johnston, K. Kieling, M. Pant, T. Rudolph, J. Smith, C. Sparrow, and M. D. Vidrighin, Creation of entangled photonic states using linear optics, arXiv:2106.13825.
[37] T. Walker, K. Miyanishi, R. Ikuta, H. Takahashi, K. Vartabi Samir, Y. Tsujimoto, K. Hayasaka, T. Yamamoto, N. Imoto, and M. Keller, Long-distance single photon transmission from a trapped ion via quantum frequency conversion, Phys. Rev. Lett. **120**, 203601 (2018).
[38] P. Kobel, M. Breyer, and M. Köhl, Deterministic spin-photon entanglement from a trapped ion in a fiber Fabry–Perot cavity, npj Quantum Inf. **7**, 6 (2021).
[39] B. Rodiek, M. Lopez, H. Hofer, G. Porrovecchio, M. Smid, X.-L. Chu, S. Gotzinger, V. Sandoghdar, S. Lindner, C. Becher, and S. Kuck, Experimental realization of an absolute single-photon source based on a single nitrogen vacancy center in a nanodiamond, Optica **4**, 71 (2017).
[40] P. Senellart, G. Solomon, and A. White, High-performance semiconductor quantum-dot single-photon sources, Nat. Nanotechnol. **12**, 1026 (2017).
[41] H. Shibata, K. Shimizu, H. Takesue, and Y. Tokura, Superconducting nanowire single-photon detector with ultralow dark count rate using cold optical filters, Appl. Phys. Express **6**, 072801 (2013).
[42] F. Marsili *et al.*, Detecting single infrared photons with 0.93 system efficiency, Nat. Photon. **7**, 210 (2013).
[43] S. Wang *et al.*, Twin-field quantum key distribution over 830-km fibre, Nat. Photon. **16**, 154 (2022).
[44] C. Weedbrook, S. Pirandola, R. Garcia-Patron, N. J. Cerf, T. C. Ralph, J. H. Shapiro, and S. Lloyd, Gaussian quantum information, Rev. Mod. Phys. **84**, 621 (2012).
[45] S. L. Braunstein and P. van Loock, Quantum information with continuous variables, Rev. Mod. Phys. **77**, 513 (2005).
[46] A. Ferraro, S. Olivares, and M. Paris, Gaussian States in Quantum Information, Napoli Series on Physics and Astrophysics (2005).
[47] B. Gupt, J. Izaac, and N. Quesada, The Walrus: A library for the calculation of hafnians, Hermite polynomials and Gaussian boson sampling, J. Open Source Softw. **4**, 1705 (2019).
[48] N. Nickerson, Y. Li, and S. Benjamin, Topological quantum computing with a very noisy network and local error rates approaching one percent, Nat. Commun. **4**, 1756 (2013).
[49] N. H. Nickerson, J. F. Fitzsimons, and S. C. Benjamin, Freely scalable quantum technologies using cells of 5-to-50 qubits with very lossy and noisy photonic links, Phys. Rev. X **4**, 041041 (2014).
[50] E. T. Campbell and S. C. Benjamin, Measurement-based entanglement under conditions of extreme photon loss, Phys. Rev. Lett. **101**, 130502 (2008).
[51] S. de Bone, P. Möller, C. Bradley, T. Taminiau, and D. Elkouss, Thresholds for the distributed surface code in the presence of memory decoherence, AVS Quantum Sci. **6**, 033801 (2024).
[52] P. Caspar, E. Verbanis, E. Oudot, N. Maring, F. Samara, M. Caloz, M. Perrenoud, P. Sekatski, A. Martin, N. Sangouard, H. Zbinden, and R. T. Thew, Heralded distribution of single-photon path entanglement, Phys. Rev. Lett. **125**, 110506 (2020).
[53] M. Takeoka, M. Sasaki, and N. Lütkenhaus, Binary projective measurement via linear optics and photon counting, Phys. Rev. Lett. **97**, 040502 (2006).